J Mater Sci: Mater Electron **(2023) 34:2283**

Structural and magnetic properties of SmCo/Co nanocomposites elaborated using sol–gel auto-combustion strategy

Sayed Emira[1,*], E. R. Shaaban[2], Shaker A. Gelany[1], and M. M. Rashad[3]

[1] *National Institute of Standards (NIS), Tersa St, El-Haram, Giza, Egypt*
[2] *Physics Department, Faculty of Science, Al-Azhar University, Assiut Branch, Assiut, Egypt*
[3] *Central Metallurgical Research and Development Institute (CMRDI), Helwan, Cairo, Egypt*

Received: 20 September 2023
Accepted: 16 November 2023
Published online: 12 December 2023

ABSTRACT

Sm–Co nanomagnetic material has received much attention recently since it is thought to be the next generation of permanent magnets with potential uses in energy technologies. Here, ethylenediaminetetraacetic acid (EDTA) is utilized for the first time as a fuel source in a sol–gel auto-combustion process to synthesize Sm–Co nanoparticles. Then, reduction–diffusion process strategy followed the auto-combustion pathway. Typically, Sm_2O_3 and Co_3O_4 nanoparticles were prepared by combining Sm and Co nitrates with the chelating agent EDTA. The Sm–Co nanocomposites were subsequently created by reductively annealing precursor oxides using calcium powder. To display the temperature-dependent breakdown of the original precursor and determine the correct annealing temperature, TGA was employed to identify the annealing temperature and the precursor products. Additionally, other physical characterization techniques such as XRD, FE-SEM, EDX, and VSM were used for further investigations. Three distinct Sm_1Co_x compositions with different cobalt ratios ($x = 4.0$, 3.5, and 2.0) were prepared and studied. The findings demonstrate that the composition Sm_1Co_x ($x = 2.0$) led to the formation of hard phases of $SmCo_5$, Sm_2Co_7, and Sm_2Co_{17}. These particles' morphology reveals that they are made up of nanowires with an average thickness of 25 nm. As well, according to the VSM findings, this composite had the highest coercivity H_c and a maximum squareness ratio M_r/M_s, which were 2161 Oe and 0.57, respectively.

1 Introduction

Permanent magnets play a vital role in many contemporary technologies and scientific areas. They are essentially used in wind turbine generators, motors, electrical vehicles, and electronic devices as well as biomedicine, hyperthermia, and even in modern advancements of mass metrology [1–7].

Sm–Co permanent magnets, e.g., Sm_2Co_{17}, have a high Curie temperature ($T_c \sim 825$ °C) as well as low

Address correspondence to E-mail: ph_sayed2014@yahoo.com

https://doi.org/10.1007/s10854-023-11658-2

remanence temperature coefficient (0.03% C^{-1}), high magnetocrystalline anisotropy, and high coercivity force [8]. These aspects give Sm–Co permanent magnets the preference to be utilized with high-temperature applications [9, 10]. Nevertheless, the scarceness and the high cost of rare earth elements, such as Sm, limited these applications.

Recently, extensive research efforts have been performed to improve the physical properties of rare-earth-transitional-metal (RE-TM) permanent magnets for high-temperature applications, in addition to developing novel permanent magnetic materials that contain fewer rare earth elements [11–13]. One of the technical methods to improve the magnetic characteristics of a permanent magnet, including high energy product and large coercivity force as well as enhanced thermal stability, is by controlling the grain size. The coercivity force is related to the magnet microstructure. When the grain is reduced to the nanometer scale, high coercivity is produced. Nanocomposites magnetic materials have demonstrated new opportunities for exploring the next generation of permanent magnets with less expensive rare-earth elements [14–19]. This will make the devices that employ this magnet more compact, lighter, and highly effective, especially in particular applications of some precise instruments such as the Kibble balance experiment. The Kibble balance experiment is used to redefine the unit of mass, the kilogram, by determining the Planck constant and requires large amounts of Sm_2Co_{17} permanent magnet [20].

Numerous approaches including physical and chemical strategies are utilized to synthesize the magnetic nanoparticles (MNPs) [21]. The physical methods are dependent on a top-down process by reducing material from bulk to micrometric or nanometric scale such as high-energy ball milling (HEBM) [22], laser deposition [23], thermal evaporation [24], and melt spinning [25]. The disadvantages of these processes are high cost, time, and energy-consuming, as well as the difficulty of controlling the grain size [26, 27]. Therefore, the problem of fabricating high-performance nanomagnetic material is affirmed.

In contrast, the chemical methods follow bottom-up processes such as co-precipitation [28], the hydrothermal method [29], oxidation synthesis [30], and the sol–gel method [31]. These chemical synthesis methods allow for more control over the microstructure such as the size and shape, crystallinity, and magnetic properties of the magnetic nanoparticles. Among these techniques, the sol–gel method is a suitable route for the preparation of monodispersed and uniform nanoparticles as well as the synthesis of RE-TM precursor. Moreover, the sol–gel method is cost-effective, facile operation, and time-saving.

When preparing RE-TM magnetic nanocomposites, e.g., SmCo, by chemical approach, commonly it requires two stages. The first stage involves the preparation of a precursor oxide, such as samarium oxide. Then, the samarium oxide must be subjected to annealing at temperatures exceeding 1000 ℃ to reduce it to Sm metallic. This conversion process is essential because Sm possesses a substantially negative reduction potential and a low free energy for oxidation. The reduction–diffusion process, which involves using a reducing agent such as calcium (Ca), allows its reduction at temperatures less than 1000 ℃ [10].

Herein, SmCo/Co nanocomposites were synthesized using the sol–gel auto-combustion method with EDTA for the first time followed by a reduction–diffusion process. In this route, EDTA was used as a fuel to generate nanocomposites with low crystallite size. Three samples with different Sm_1Co_x compositions of [(I) $x = 4.0$, (II) $x = 3.5$, and (III) $x = 2.0$] were prepared and studied. The synthesis process involves two steps. The first step is to prepare the precursor oxides SmCo–O particles, which contain Sm_2O_3 and Co_3O_4. Subsequently, the reduction–diffusion process was carried out by mixing the precursor oxides with Ca and KCl under high temperature in high-purity argon gas. Finally, the product was washed to produce the particles of SmCo/Co nanocomposites.

As a result, nanoparticles with different phase structures were formed. The morphology of the produced nanoparticles was studied and verified. The sample with Sm_1Co_x composition of $x = 2.0$ had the highest coercivity value of 2161 Oe with a maximum squareness ratio of 0.57.

2 Experimental

2.1 Chemicals

Samarium (III) nitrate hexahydrate [$Sm(NO_3)_3{\cdot}6H_2O$, 99.9%, Sigma-Aldrich], cobalt(II) nitrate hexahydrate [$Co(NO_3)_2{\cdot}6H_2O$, ≥ 98%, Sigma-Aldrich], Ethylenediaminetetraacetic acid ($C_{10}H_{16}N_2O_8$, 99%, Sigma-Aldrich), calcium granular (Ca, granular

99%, Sigma-Aldrich), and potassium chloride (KCl, 99.0–100.5%, Sigma-Aldrich).

2.2 Synthesis of precursors (Sm–Co oxides)

The synthesis process of Sm–Co nanoparticles is summarized in Fig. 1.

In order to synthesize Sm–Co particles oxide, samarium (III) nitrate hexahydrate and cobalt (II) nitrate hexahydrate were used to synthesize the precursors with different molar ratios. Three samples were synthesized according to the following Sm_1Co_x compositions of [(I) $x = 4.0$, (II) $x = 3.5$, and (III) $x = 2.0$]. The samples were dissolved in 100 ml of deionized water with mechanical stirring. Then EDTA was inserted to the solution with a molar ratio of 2:1, respectively. The advantage of using EDTA is that it can chelate the most of metals ions based on four carboxylate groups that are cross-linked easily to create a gel [32]. The mixed solution was heated at temperatures of 80–90 ℃ until the solvent evaporated and produced a viscous gel. Subsequently, the temperature of the formed gel was increased up to 300 ℃ to perform the combustion process. After cooling to room temperature, the samples were collected and crushed to obtain the powder. To prepare pure oxides of SmCo, the sample powders were annealed at 800 ℃ (which was chosen based on TGA analysis) for 2 h in atmospheric air. The resulting black powder for the three samples was collected and kept for the following reductive annealing.

2.3 Synthesis of SmCo/Co nanocomposites

After the precursor oxides were prepared, a mixture of 1 g of the precursor with 5 g of calcium (Ca) granular as a reducing agent and 3 g of potassium chloride powder (KCl) as a solvent was combined. Then this mixture was placed in a boat made from alumina. This boat was transferred to a tube furnace and annealed at a temperature of 900 ℃ for 2 h under a flowing high-purity argon atmosphere. The boat was kept inside the furnace until it cooled to ambient environmental temperature. In order to dissolve and remove CaO, KCl, extra Ca, and other impurities, a diluted hydrochloric acid was used to wash the products. To ensure that all of the impurities were removed, the washing process was repeated multiple times using deionized water. The final black powder was collected by a magnet and stored for further characterization.

2.4 Physical properties

The thermogravimetric analysis (TGA) (Shimadzu 50 with an accuracy of 0.1 K) was realized to analyze the precursor products in order to track the temperature-dependent breakdown of the original precursor and establish the proper annealing temperature. In an environment of air, the temperature was raised from room temperature up to 800 ℃ with a heating rate of 10 ℃/min. The crystallographic characteristics of the samples were identified by using X-ray diffractometer (Malvern Panalytical) with CuKα radiation at a wavelength of 1.540595 Å. All of the samples were tested in continuous mode from 20 to 80° at room temperature.

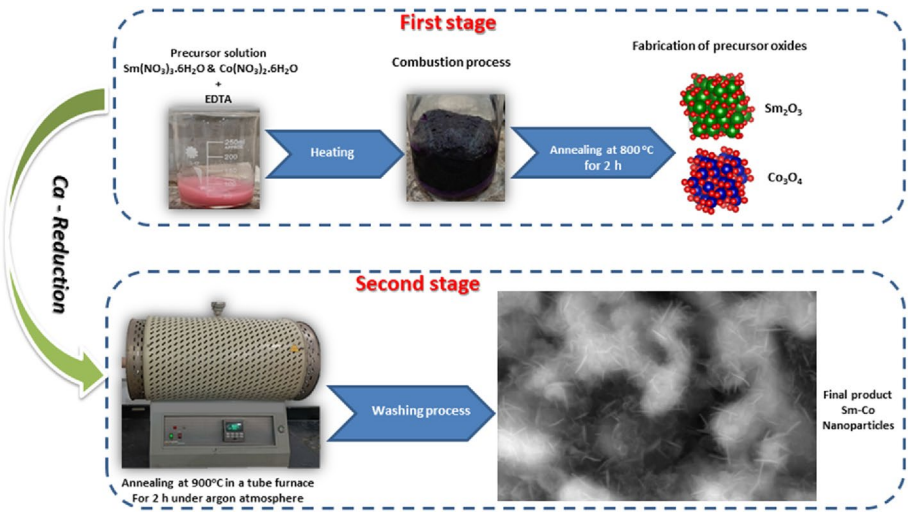

Fig. 1 A schematic illustration representing the process of synthesis

The size, morphologies, and elemental analysis of the produced nanoparticles were verified using field emission scanning electron microscope equipped with energy-dispersive X-ray spectroscopy (FE-SEM; Quattro S, Thermo Scientific). Moreover, the hysteresis loops and magnetic properties were measured using a vibrating sample magnetometer (VSM, Lake Shore Co., model 7400-1, USA) at room temperature with a maximum applied field strength of 20 kOe.

3 Results and discussion

3.1 Phase structural of precursor powder

Preparing the Sm–Co oxide phase is the first stage in synthesizing SmCo/Co nanocomposites. To show the changes that occurred during the heat treatment of the precursor powders, the TGA analysis for precursor of sample (III) (of Sm_1Co_x composition of $x = 2.0$) was performed from room temperature to 800 ℃ with a heating rate of 10 ℃/min in Air, Fig. 2. As given in Fig. 2, the TGA curve of weight loss performs through three stages. The first stage, which occurred in the temperature range of 30–130 ℃, presented a weight loss of roughly 10 wt% and was attributable to the elimination of adsorbed water. When the temperature was between 130 and 340 ℃, the majority of the organic materials were destroyed with a second weight loss of roughly 57 wt%. The third step indicated the ultimate decomposition of the NO_3 group. All of the organics were ejected due to the precursors' decomposition tendency, and Sm_2O_3–Co_3O_4 phases were produced instead. At temperatures below 800 ℃, there was an approximate 71% overall weight reduction. To ensure that all the organics broke down, 800 ℃ was selected as the annealing temperature.

To verify the TGA results mentioned above, Fig. 3 shows the XRD pattern for sample (III) of Sm_1Cox composition of $x = 2.0$, which was annealed at 800 ℃ for 2 h in the atmosphere. The XRD pattern shows that the phases formed consisted of Sm_2O_3 (JCPDS No. 070-2642) and Co_3O_4 (JCPDS No. 074-1657).

The average crystallite size of the oxide powder product was estimated from the Scherrer's Eqs. [33–35]:

$$D = \frac{K\lambda}{\beta \cos\theta}, \tag{1}$$

where D is the average crystallite size in nm, K is the Scherer constant, $K = (0.89)$, λ is the X-ray diffraction wavelength of Cu-Kα line ($\lambda = 1.5406$ Å), β is the full width at half maximum (FWHM) in radians, and θ is the Bragg angle.

The results obtained show that both Sm_2O_3 and Co_3O_4 particles have a good crystallinity with a small average crystallite size of 21 and 22 nm, respectively.

3.2 Crystal structure of SmCo/Co nanocomposites

Figure 4 shows the XRD patterns of Sm–Co nanoparticles synthesized at different compositions of Sm:Co (denoted I, II, and III). The sample (I) with a Sm:Co ratio of 1:4.0 confirms that the formation of the

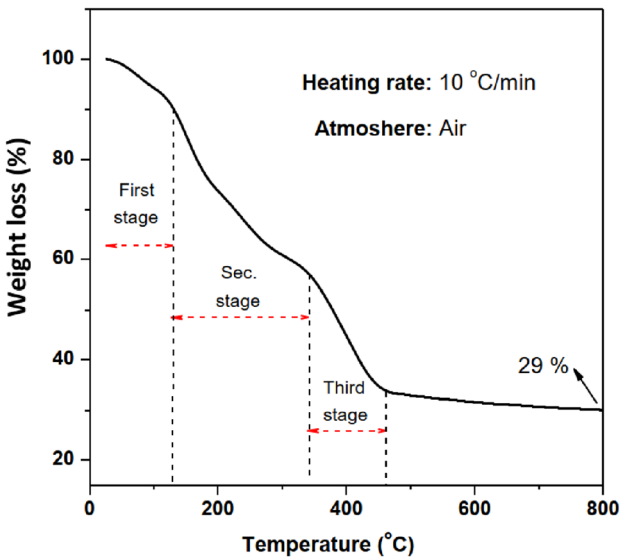

Fig. 2 Thermogravimetric analysis of the precursor oxides

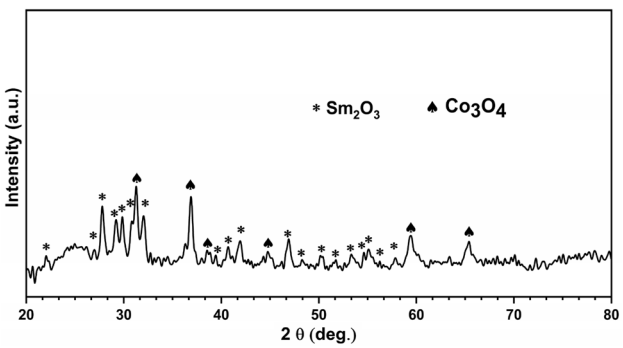

Fig. 3 XRD pattern of the precursor oxides

hexagonal $SmCo_5$ phase (JCPDS No. 065-8981) was formed with average crystallite size of 35 nm estimated by the Scherrer formula, Fig. 4a. Moreover, the presence of Co (JCPDS No. 96-901-1625 and JCPDS No. 001-1254) and Sm_2O_3 phases (JCPDS No.013-0244) were revealed with average crystallite sizes of 19 and 29 nm, respectively.

By reducing the Sm:Co ratio to 1:3.5 (sample II), hexagonal Sm_2Co_{17} phase (JCPDS No. 035-1368) and cubic Co phase (JCPDS No. 089-7093) were formed with average crystallite size of 24 and 23 nm, respectively, Fig. 4b. The two samples (I and II) show the formation of the Co phase as the major synthesized phase.

In order to achieve the majority formation of the SmCo phase, the Co ratio was decreased in sample III to 1:2.0 of Sm:Co ratio. Therefore, Fig. 4c shows the typical diffraction peaks of hexagonal $SmCo_5$ (JCPDS No. 056-0085) such as (111) and (101). Furthermore, a hexagonal Sm_2Co_7 (JCPDS No. 056-3640), rhombohedral Sm_2Co_{17} (JCPDS No. 019-0359) phases, and a few diffraction peaks of cubic Co phase (JCPDS No. 900-8467) were formed. Sm–Co permanent magnets commonly possess a number of stable binary equilibrium phases, such as $SmCo_5$, Sm_2Co_{17}, Sm_2Co_7, and $SmCo_3$. Among the various phases produced with chemical synthesis, $SmCo_5$ and Sm_2Co_{17} possess large magnetocrystalline anisotropy and superior magnetic properties [36]. The average crystallite size was estimated to be 18, 25, 23, and 24 nm for the previous formation phases, respectively.

The discrepancies between the Sm:Co ratios in the actually prepared samples and those in theory are imputed to the possibility of evaporating and oxidizing a fraction of Sm meanwhile the synthesis process [37]. Besides, Sm_2O_3 did not achieve a full reaction with Co in the process of reduction, resulting in a trace of the Sm_2O_3 phase observed in the XRD pattern, Fig. 4a.

The possible reaction mechanism during the preparation process can be explained as follows [19, 38]:

$$\mathrm{Sm(NO_3)_3 \cdot 6H_2O + Co(NO_3)_2 \cdot 6H_2O + 2EDTA \rightarrow Sm_2CO_3(EDTA)_2 + 12H_2O + 5HNO_3} \quad (2)$$

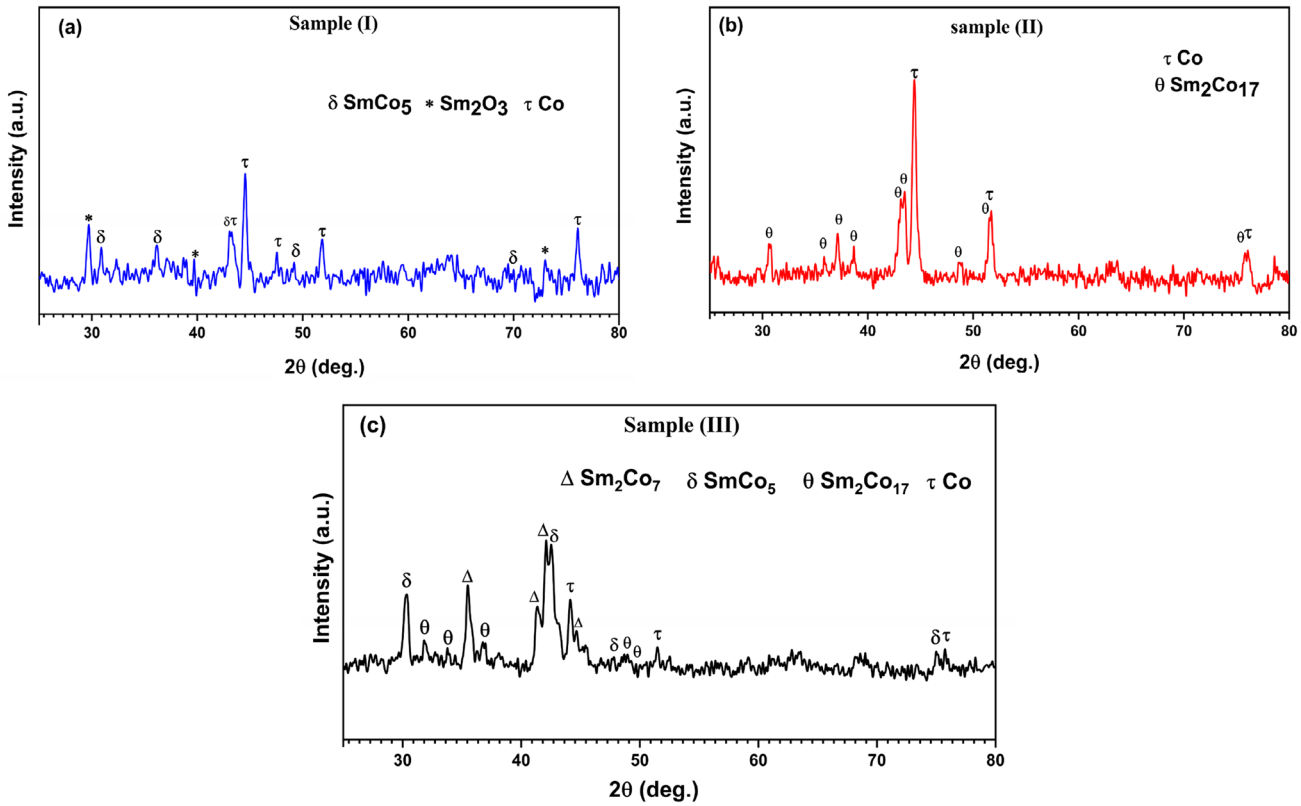

Fig. 4 The XRD patterns of the final produced powder of the samples with Sm:Co ratios of **a** 1:4.0, **b** 1:3.5 and **c** 1:2.0

$$Sm_2CO_3(EDTA)_2 \xrightarrow{800^{\circ}C(air)} Sm_2O_3 + Co_3O_4 + 16H_2O\uparrow + 6NO_2\uparrow + 20CO_2\uparrow \quad (3)$$

$$Sm_2O_3 + Co_3O_4 + Ca + KCl \xrightarrow{900^{\circ}C(argon)} SmCo\ (\text{with different ratios}) + Co + 7CaO \quad (4)$$

3.3 Microstructural observations

Figure 5 presents the field emission-scanning electron microscope (FE-SEM) micrographs of the produced powder after the reduction and washing process for the three samples. The morphology of Sm–Co particles, size distribution, and elemental distribution were investigated.

The particles of sample (I) are observed in the form of nanoplates with an average thickness of 43 nm, as shown in Fig. 5a, d. Samples (II) and (III); in contrast to sample (I), the particles of these samples are composed in the form of nanowires. Sample (II) has a diameter size distribution in the range of 27 nm, as shown in Fig. 5b, e. The sample (III) has a slightly smaller diameter size distribution, ranging around 25 nm, as depicted in Fig. 5c, f.

Furthermore, the samples had a certain degree of aggregation of the particles. The annealing process can lead to this aggregation of particles in the samples. Additionally, during the washing process of Sm–Co nanoparticles, various treatment solutions can be used. The choice of treatment solutions and their properties can influence the final surface characteristics of

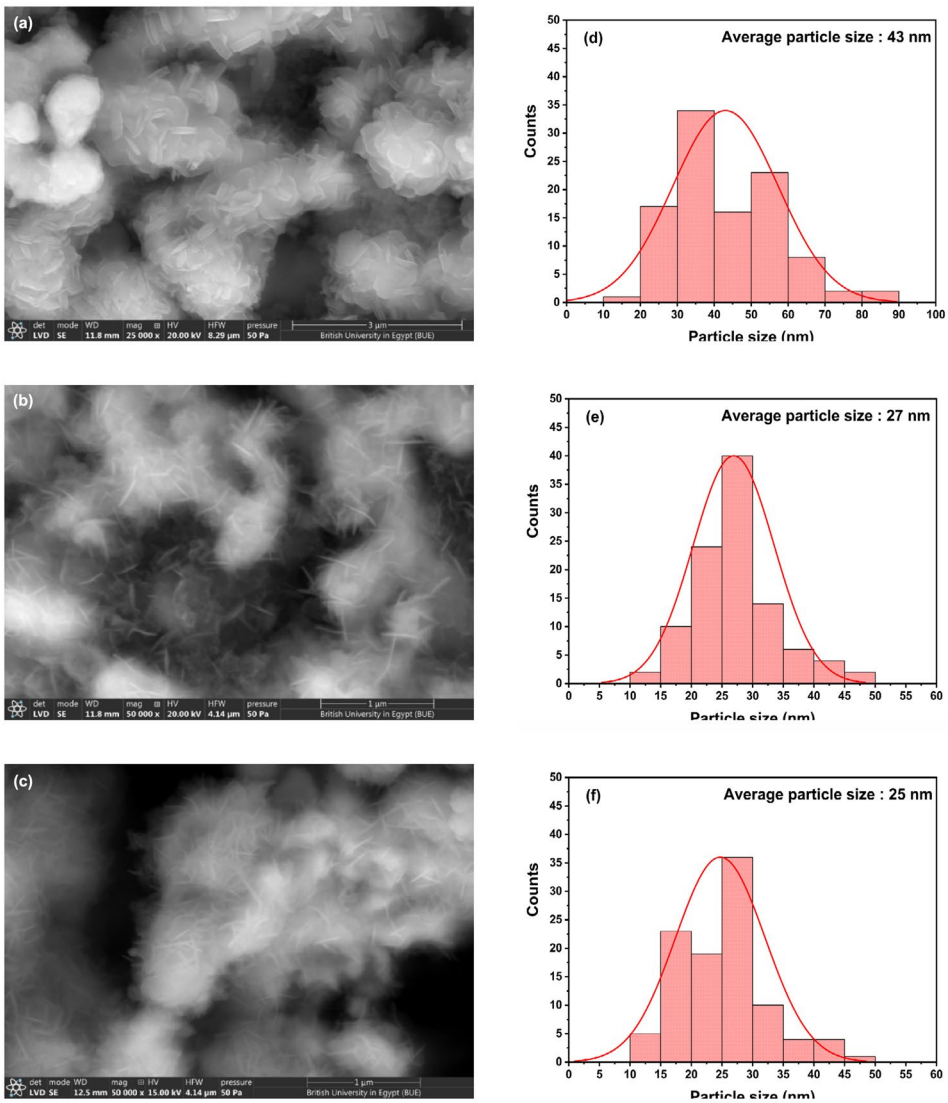

Fig. 5 **a**, **b**, **c** FE-SEM micrographs of the samples with Sm:Co ratios of 1:4.0 (I), 1:3.5 (II), and 1:2.0 (III); **d**, **e**, **f** the average particle size distribution

the nanoparticles [39]. It is notable that the crystallite size obtained from XRD patterns is close to the average particle size extracted from FE-SEM images.

The EDX measurements were carried out to verify the presence of the different elements in the samples and the results are illustrated in Fig. 6. EDX results showed the presence of samarium and cobalt, which represent the main elements of the samples. For sample (I) with Sm_1Co_x ratio of $x = 4$ and additional peak of O was observed in the EDX spectrum, Fig. 6a.

3.4 Magnetic properties

The magnetic coercivity of materials depends on several parameters including phase composition, impurity phases, crystallinity, and are directly related to particle size. When the particle size decreases, it usually leads to decreases in the magnetic properties. Due to the decreasing particle size, the magnetic anisotropy energy for particles responsible for holding the magnetic moment along specific directions becomes weak [36]. In contrast, the coercivity reaches its maximum value at a critical domain size which is equal to the size of a single domain [40]. The critical size of a single magnetic domain for different types of Sm–Co such as Sm_2Co_7, $SmCo_5$, and Sm_2Co_{17} is about 1600, 1120, and 550 nm, respectively [41].

Figure 7 depicts the magnetic hysteresis loops (M–H) of the three samples measured at room temperature with an applied magnetic field of 20 kOe. It is observed that all the samples demonstrated ferromagnetic behavior.

The magnetic parameters involving the coercivity (H_c), the saturation magnetization (M_s), the remanence magnetization (M_r), and the squareness ratio (M_r/M_s) ratio were extracted and listed in Table 1.

As presented, sample (I) has low H_c and high M_S values which could be due to the existence of the Sm_2O_3 impurity phase and the presence of soft magnetic phase Co. Sample (II) has the majority of Co phase with small particle size, this reduced H_c and M_s values to 729 Oe and 64.52 emu/g, respectively, despite the formation of Sm_2Co_{17} phase. In sample (III), the reduction of Co ratio resulted in the formation of majority phases of SmCo and a low Co soft phase. This led to an improvement in the coercivity value H_c and reached the highest value of 2161 Oe among the three samples. Meanwhile, this sample exhibited a maximum squareness ratio M_r/M_s of 0.57, which was the highest among all the other samples. The variations of magnetic properties with respect to the cobalt ratio are presented in Fig. 8. Furthermore, the observed decrease in saturation magnetization for sample (III) was most likely attributed to the decrease in crystallinity as well as particle size.

Further investigations can be conducted to optimize the magnetic properties by studying the effects of annealing time and annealing temperature as well as further controlling the Co/Sm ratio [10, 27, 42].

4 Conclusion

In this study, the sol–gel auto-combustion method and the reduction–diffusion strategies were combined to create Sm–Co nanoparticles. For instance, three samples of Sm_1Co_x compositions with different cobalt ratios ($x = 4.0$, 3.5, and 2.0) were prepared. The precursor oxides were successfully tailored using Sm and Co nitrates with EDTA as a fuel for the first time. EDTA has the advantage of chelating most metals that are cross-linked easily to form a gel related to four carboxylate groups. The precursor powders were considered and depicted the formation of Sm_2O_3 and Co_3O_4 phases with good crystallinity. SmCo/Co nanocomposites were obtained after the reduction–diffusion process utilizing Ca as a reducing agent. The thermogravimetric analysis evinced the proper annealing temperature 800 ℃ to form metal oxide components. Additionally, XRD, FE-SEM, EDX, and VSM were used to analyze the structure, shape, size, elemental analysis, and magnetic characteristics of the produced particles.

When adjusting the Sm and Co ratio to 1:2.0 in precursor compounds, permanent magnetic phases of $SmCo_5$, Sm_2Co_7, and Sm_2Co_{17} were acquired. The microstructures of these particles displayed a nanowire-like structure with an average diameter of 25 nm. Furthermore, magnetic measurements revealed that this sample had the highest coercivity H_c of 2161 Oe and a maximum squareness ratio M_r/M_s of 0.57.

Author contributions

All authors have contributed to the design and implementation of the research, discussed the results, writing of the manuscript, and approved the final manuscript.

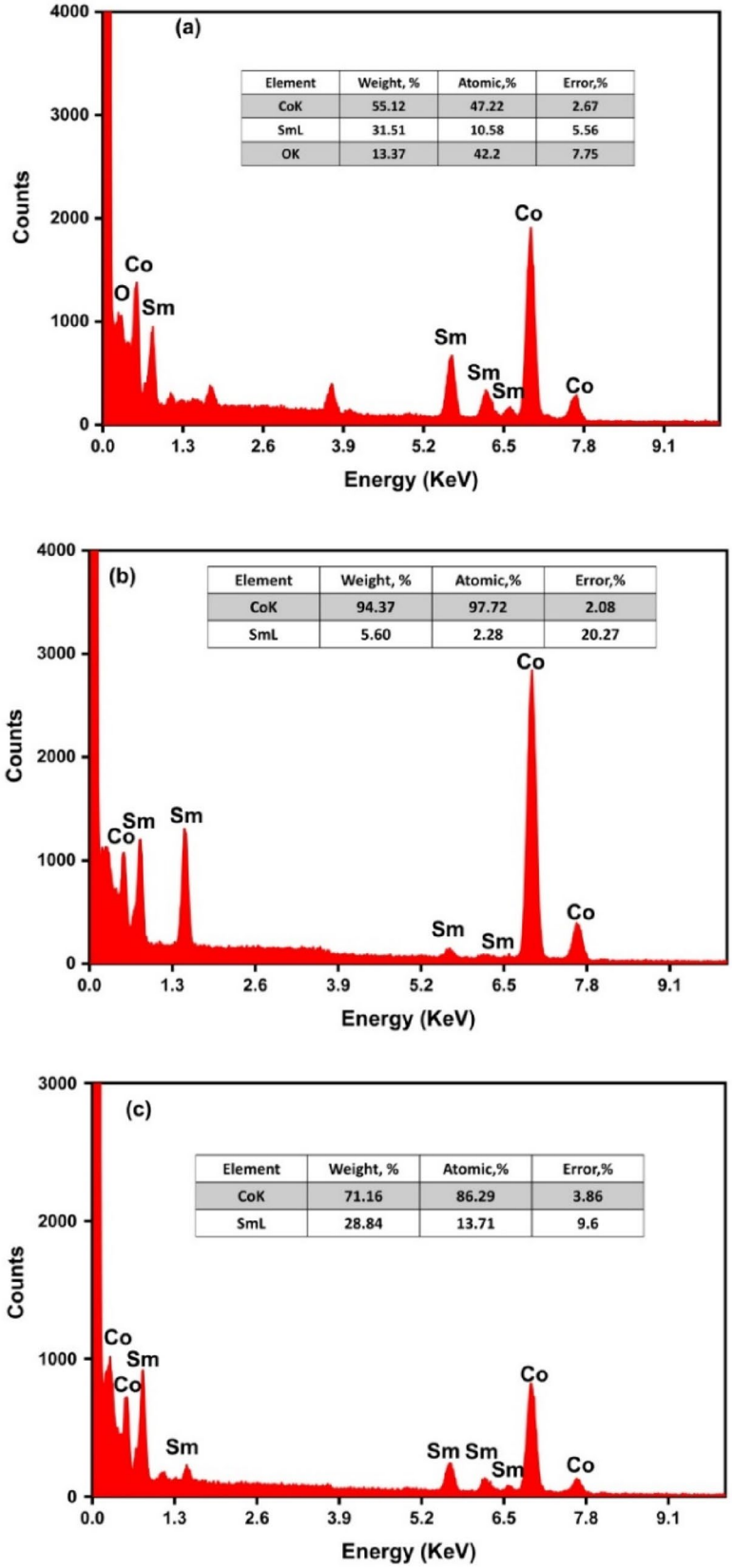

Fig. 6 EDX spectra of the samples Sm_1Co_x compositions of **a** $x=4.0$, **b** $x=3.5$, and **c** $x=2.0$

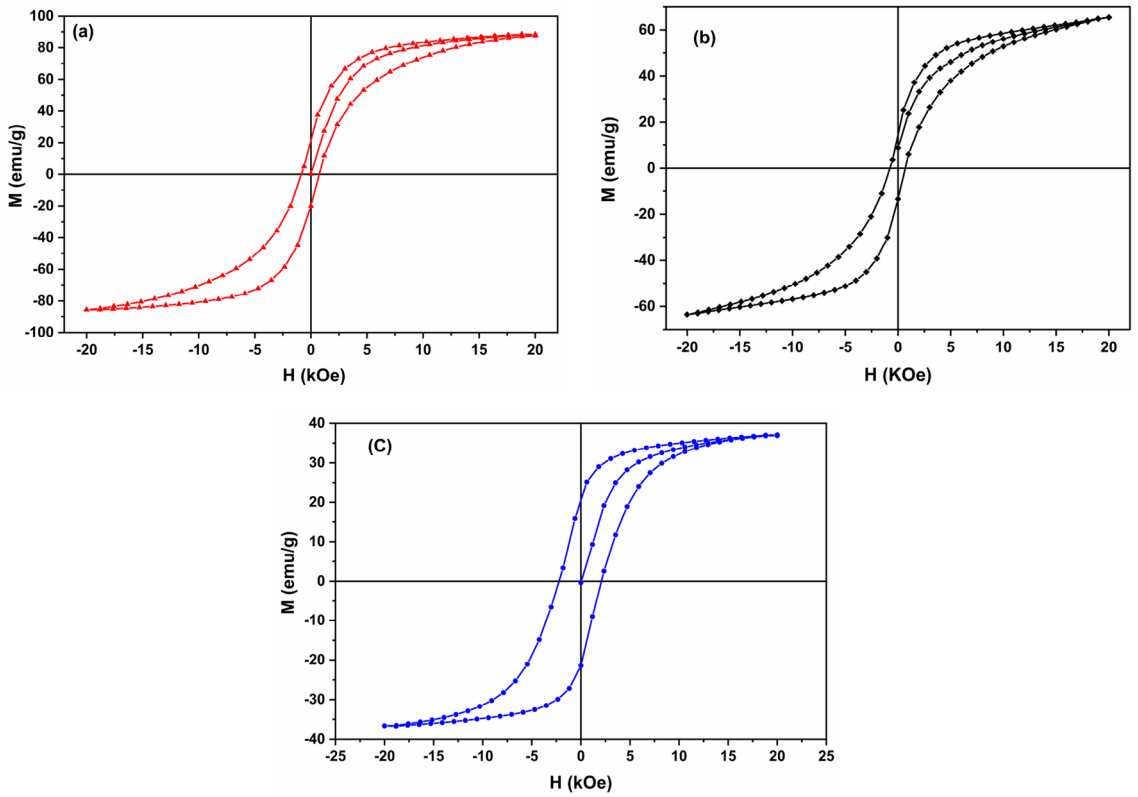

Fig. 7 The *M–H* hysteresis loops of the reduced and washed samples with Sm_1Co_x compositions of **a** $x=4.0$, **b** $x=3.5$, and **c** $x=2.0$

Table 1 The magnetic properties of the reduced samples after washing procedures

Sample	Sm:Co ratio	Coercivity H_c(Oe)	Saturation magnetization (M_s) (emu/g)	Remanent magnetization (M_r) (emu/g)	Squareness ratio $(M_{rs})=M_r/M_s$
I	1:4.0	797	86.96	20.67	0.24
II	1:3.5	729	64.52	13.94	0.22
III	1:2.0	2161	36.91	20.96	0.57

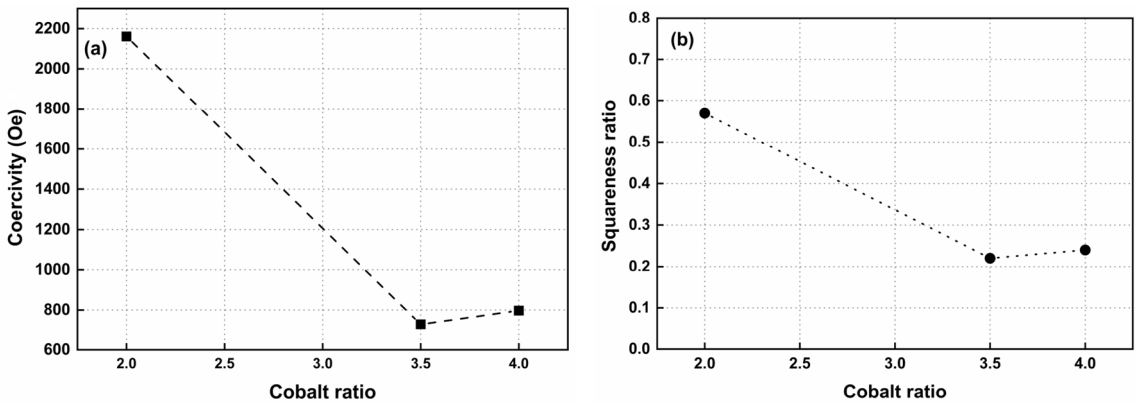

Fig. 8 The effect of Co ratio on **a** coercivity and **b** squareness ratio of the samples

Funding

Open access funding provided by The Science, Technology & Innovation Funding Authority (STDF) in cooperation with The Egyptian Knowledge Bank (EKB). Open access funding was provided by The Science, Technology & Innovation Funding Authority (STDF) in cooperation with The Egyptian Knowledge Bank (EKB).

Data availability

This article contains all of the data collected during this study.

Declarations

Conflict of interest The authors declare that they have no conflicts of interest.

References

1. J. Croat, J. Ormerod, *Modern permanent magnets*, 1st edn. (Woodhead Publishing, Elsevier, 2022), p.403
2. H. Wang, T. Lamichhane, M. Paranthaman, Review of additive manufacturing of permanent magnets for electrical machines: a prospective on wind turbine. Mater. Today Phys. **24**, 100675 (2022). https://doi.org/10.1016/j.mtphys.2022.100675
3. J. Cui, J. Ormerod, D. Parker, R. Ott, A. Palasyuk, S. Mccall, M. Paranthaman, M. Kesler, M. Mcguire, I. Nlebedim, C. Pan, T. Lograsso, Manufacturing processes for permanent magnets: part I—sintering and casting. JOM **74**, 1279–1295 (2022). https://doi.org/10.1007/s11837-022-05156-9
4. J. Chen, L. Rissing, Electroplating hard magnetic SmCo for magnetic microactuator applications. J. Appl. Phys. **109**, 07A766 (2011). https://doi.org/10.1063/1.3565414
5. O. Gutfleisch, M. Willard, E. Brück, C. Chen, S. Sankar, J.P. Liu, Magnetic materials and devices for the 21st century: stronger, lighter, and more energy efficient. Adv. Mater. **23**, 821–842 (2011). https://doi.org/10.1002/adma.201002180
6. H. Rui, R. Xing, Z. Xu, Y. Hou, S. Goo, S. Sun, Synthesis, functionalization, and biomedical applications of multifunctional magnetic nanoparticles. Adv. Mater. **22**, 2729–2742 (2010)
7. S.S. Li, Z.H. Zhang, W. Zhao, Z.K. Li, S.L. Huang, Progress on accurate measurement of the Planck constant: Watt balance and counting atoms. Chinese Phys. B **24**(1), 010601 (2015)
8. J. Yi, Development of samarium–cobalt rare earth permanent magnetic materials. Rare Met. **33**, 633–640 (2014)
9. T. Zhang, H. Liu, J. Liu, C. Jiang, 2:17-type SmCo quasi-single-crystal high temperature magnets. Appl. Phys. Lett. **106**, 162403 (2015). https://doi.org/10.1063/1.4918939
10. J. Park, H. Kwon, J. Park, J. Ro, S. Suh, Synthesis and characterization of Sm_2Co_{17} using electrodeposition and reduction-diffusion process. J. Alloys Compd. **901**, 163669 (2022). https://doi.org/10.1016/j.jallcom.2022.163669
11. C. Jiang, S. An, Recent progress in high temperature permanent magnetic materials. Rare Met. **32**, 431–440 (2013)
12. B. Jiang, L. Lian, Y. Xing, N. Zhang, Y. Chen, P. Lu, D. Zhang, Advances of magnetic nanoparticles in environmental application: environmental remediation and (bio)sensors as case studies. Environ. Sci. Pollut. Res. **25**, 30863–30879 (2018). https://doi.org/10.1007/s11356-018-3095-7
13. S. Liu, Sm–Co high-temperature permanent magnet materials. Chin. Phys. B **28**(28), 017501 (2019)
14. K. Guo, H. Lu, G.J. Xu, D. Liu, H.B. Wang, X.M. Liu, X.Y. Song, Recent progress in nanocrystalline Sm–Co based magnets. Mater. Today Chem. **25**, 100983 (2022). https://doi.org/10.1016/j.mtchem.2022.100983
15. M. Hu, H. Zhang, Perspective and prospects for nanostructured magnets. J. Appl. Phys. **133**, 170901 (2023). https://doi.org/10.1063/5.0149640
16. J. Xu, K. Zhu, S. Gao, Rare earth permanent magnetic nanostructures: chemical design and microstructure control

to optimize magnetic properties. Inorg. Chem. Front. **8**, 383–395 (2021)
17. M. Yue, X. Zhang, J.P. Liu, Fabrication of bulk nanostructured permanent magnets with high energy density: challenges and approaches. Nanoscale **9**, 3674–3697 (2017)
18. K. Yang, X. Liu, Y. Zhang, Z. Ma, The chemical fabrication of heterostructured $SmCo_5$/Fe nanocomposites. J. Mater. Sci. Mater. Electron. **33**, 20439–20446 (2022). https://doi.org/10.1007/s10854-022-08859-6
19. J. Lee, T. Hwang, M. Kang, G. Lee, H. Cho, J. Kim, Y. Choa, High-performance, cost-effective permanent nanomagnet: microstructural and magnetic properties of Fe-substituted SmCo nanofibe. Appl. Surf. Sci. J. **471**, 273–276 (2019). https://doi.org/10.1016/j.apsusc.2018.11.217
20. I. Robinson, S. Schlamminger, The Watt or Kibble balance: a technique for implementing the new SI definition of the unit of mass. Metrologia **53**, A46–A74 (2016)
21. A. El-Gendy, J. Barandiarán, R. Hadimani, Magnetic Nanostructured Materials From Lab to Fab, 1st edn. (Elsevier, 2018), p.1
22. A. Bajorek, P. Łopadczak, K. Prusik, M. Zubko, Correlation between microstructure and magnetism in Ball–Milled $SmCo_5$/α-Fe (5%wtα-Fe) nanocomposite magnets. Materials **14**(4), 1–20 (2021). https://doi.org/10.3390/ma14040805
23. V. Neu, J. Thomas, S. Fähler, B. Holzapfel, L. Schultz, Hard magnetic SmCo thin films prepared by pulsed laser deposition. J. Magn. Magn. Mater. **242–245**, 1290–1293 (2002). https://doi.org/10.1016/S0304-8853(01)01264-1
24. L. Castaldi, K. Giannakopoulos, A. Travlos, N. Boukos, D. Niarchos, S. Boukari, E. Beaurepaire, Engineering of FePt nanoparticles by e-beam co-evaporation. Nanotechnology **19**, 135702 (2008)
25. X. Chi, Z. Chen, S. Wang, T. Guo, J. Li, J. Sun, Y. Zhang, Microstructure and magnetic properties of $Sm_3Co_{11-x}Fe_xB_4$ ribbons with superior coercivity. J. Alloys Compd. **942**, 169107 (2023). https://doi.org/10.1016/j.jallcom.2023.169107
26. N. Poudyal, J. Liu, Advances in nanostructured permanent magnets research. J. Phys. D. Appl. Phys. **46**, 043001 (2013)
27. T. Hwan, J. Lee, M. Kang, G. Lee, J. Kim, Y. Choa, Synthesis and magnetic properties of Sm_2Co_{17} particles using salt-assisted spray pyrolysis and a reduction-diffusion process. Appl. Surf. Sci. **475**, 986–989 (2019). https://doi.org/10.1016/j.apsusc.2019.01.030
28. Y. Dong, T. Zhang, H. Wang, X. Liu, C. Jiang, Chemical synthesis and characterization of $SmCo_5$/Co magnetic nanocomposite particles. Rare Met. **40**, 1224–1231 (2021). https://doi.org/10.1007/s12598-020-01640-w
29. B. Sun, Y. Liu, W. Zhao, J. Wu, P. Chen, Hydrothermal preparation and white-light-controlled resistive switching behavior of $BaWO_4$ nanospheres. Nano-Micro Lett. **7**(1), 80–85 (2015). https://doi.org/10.1007/s40820-014-0021-5
30. Z. Hou, P. Yan, B. Sun, H. Elshekh, B. Yan, An excellent soft magnetic Fe/Fe_3O_4–FeSiAl composite with high permeability and low core loss. Results Phys. **14**, 102498 (2019). https://doi.org/10.1016/j.rinp.2019.102498
31. H. Tang, Z. Wang, M. Mamakhel, M. Dong, M. Christensen, Combustion assisted preparation of high coercivity Sm–Co hard magnet with stable single-domain size. J. Alloys Compd. **816**, 152527 (2020). https://doi.org/10.1016/j.jallcom.2019.152527
32. L. Klein, M. Aparicio, A. Jitianu, Handbook of Sol–Gel Science and Technology: Processing, Characterization and Applications, 2nd edn. (Springer, 2018), p.1067.
33. P. Scherrer, Bestimmung der Grösse und der inneren Struktur von Kolloidteilchen mittels Röntgenstrahlen. Nachr. Ges. Wiss. Göttingen **26**, 98 (1918)
34. J. Langford, A. Wilson, Scherrer after sixty years: a survey and some new results in the determination of crystallite size. J. Appl. Cryst. **11**, 102 (1978)
35. V. Uvarov, I. Popov, Metrological characterization of X-ray diffraction methods for determination of crystallite size in nano-scale materials. Mater. Charac. **85**, 111 (2013)
36. J. Tian, S. Zhang, X. Qu, D. Pan, M. Zhang, Co-reduction synthesis of uniform ferromagnetic SmCo nanoparticles. Mater. Lett. **68**, 212–214 (2012). https://doi.org/10.1016/j.matlet.2011.10.076
37. M. Najarzadegan, F. Karimzadeh, H.R. Salimijazi, S. Adhami, The synthesis of SmCo/Co nanoplates: reductant effect in the synthesis process. J. Sol-Gel Sci. Technol. **92**, 706–714 (2019). https://doi.org/10.1007/s10971-019-05111-2
38. J. Lee, T. Hwang, M. Kang, H. Cho, J. Kim, N. Myung, Y. Choa, Synthesis of Samarium-Cobalt sub-micron fibers and their excellent hard magnetic properties. Front. Chem. (2018). https://doi.org/10.3389/fchem.2018.00018
39. J. Lee, T. Hwang, H. Cho, J. Kim, Y. Choa, Near theoretical ultra-high magnetic performance of rare-earth nanomagnets via the synergetic combination of calcium-reduction and chemoselective dissolution. Sci. Rep. **8**, 1–11 (2018)
40. B. Shen, S. Sun, Chemical synthesis of magnetic nanoparticles for permanent magnet applications. Chem. Eur. J. **26**, 6757–6766 (2020). https://doi.org/10.1002/chem.201902916
41. Y. Dong, H. Wang, B. Liu, X. Liu, J. Shang, Z. Liu, T. Zhang, C. Jiang, Morphology evolution of $SmCo_x$ permanent magnetic nanoparticles. Sci. China-Phys. Mech.

Astron. **64**, 247511 (2021). https://doi.org/10.1007/s11433-020-1657-7

42. M. Najarzadegan, F. Karimzadeh, H. Salimijazi, S. Adhami, The effect of reduction process parameters on magnetic and structural properties of SmCo/Co nanocomposites. J. Supercond. Nov. Magn. **33**, 783–793 (2020). https://doi.org/10.1007/s10948-019-05257-8